Received: 5 January 2021 | Revised: 25 February 2021 | Accepted: 26 February 2021

DOI: 10.1002/jrs.6091

RESEARCH ARTICLE

Journal of RAMAN SPECTROSCOPY WILEY

The correlation between experimental polarized Raman spectra and their density functional theory prediction in the LCAO framework: The *R*3*c* $LiNbO_3$ crystal as a test case

Bernardo A. Nogueira[1,2] | **Alberto Milani**[2] | **Chiara Castiglioni**[2] | **Rui Fausto**[1]

[1]CQC, Department of Chemistry, University of Coimbra, Coimbra, Portugal

[2]CMIC, Dipartimento di Chimica, Materiali e Ingegneria Chimica "G. Natta", Politecnico di Milano, Milan, Italy

Correspondence
Bernardo A. Nogueira, CQC, Department of Chemistry, University of Coimbra, P-3004-535 Coimbra, Portugal.
Email: ban@qui.uc.pt

Funding information
"Fundação para a Ciência e a Tecnologia"—FCT, Grant/Award Numbers: UIDP/00313/2020, UIDB/00313/2020: SFRH/BD/129852/2017

Abstract

In this study, the polarized Raman spectra of the *R*3*c* $LiNbO_3$ crystal are used as a benchmark test for density functional theory (DFT) full periodic boundary conditions linear combination of atomic orbitals (LCAO) calculation of the Raman tensors, according to the implementation in the CRYSTAL software. The theoretical approach used proved to provide excellent results regarding wavenumbers and relative intensities predictions for the transverse optical modes of both A_1 and E symmetry, considerably improving over previously reported data based on the plane waves approach. Overall, the present investigation demonstrates that the LCAO approach, as implemented in the CRYSTAL software, gives excellent results regarding the calculation of Raman tensors and polarized Raman spectra. The possibility to put in correspondence the individual Raman tensors components and bands intensities in the different back-scattering experimental configurations revealed that the computed Raman tensors are very accurate, not only considering their average values (tensors invariant in the combination suitable for the description of Raman scattering of isotropic materials) but also when the tensors individual components are considered. Based on the present results, a reassignment of the E (TO) modes of the *R*3*c* $LiNbO_3$ crystal is proposed, in particular for the 2 E and 9 E modes, which have been a matter of discussion in the recent years.

KEYWORDS

CRYSTAL software, fully periodic LCAO, $LiNbO_3$, lithium niobate, polarized Raman

1 | INTRODUCTION

Lithium niobate ($LiNbO_3$) is a synthetic dielectric material,[1] belonging to the ferroelectric oxides class,[2] which is regularly used in various applications in nonlinear electro-optics[2–7] and acoustics,[1,8] because of its large elasto-optic, electro-optic, nonlinear optical, and piezoelectric coefficients.[1,8] At room temperature, $LiNbO_3$ exists as an uniaxial crystal that belongs to the trigonal system (space group *R*3*c* and symmetry point group 3 m), with two formula units per cell. Below the ferroelectric Curie temperature (~1210°C), the crystal structure of $LiNbO_3$ comprises planar sheets of oxygen atoms in a distorted hexagonal close-packed configuration, the octahedral interstices in the structure being filled by lithium or niobium atoms (one third each) or being vacant (one third), in a continuous intercalated sequence.[1] The compound has been extensively studied

due to the availability of large macroscopic single crystals suitable for investigation. This feature is particularly useful for polarized-light Raman experiments, and several studies on this subject have been reported.[2,5–8] Nevertheless, as discussed below in detail, there is still no consensus regarding assignment of some Raman bands to specific vibrations, and the analysis of the band intensities of the polarized-light Raman spectra of $LiNbO_3$ obtained for different geometric arrangements at the light of contemporary LCAO-based electronic structure calculations has not yet been conveyed.

In the present article, we present a comprehensive analysis of the Raman band intensities of the room temperature polarized-light Raman spectra of $LiNbO_3$ based on the detailed comparison of the experimental data with those resulting from start-of-the-art full periodic electronic structure calculations. In contrast to the standard theoretical predictions mimicking the non-polarized spectrum of an isotropic sample, where the Raman intensities are determined by averages of the elements of the polarizability tensor, we exploit here complementary experiments that probe the individual tensor components one at a time. This allows evaluating the reliability of present day density functional theory (DFT) simulations in predicting these components, as well as expanding our understanding of the experimental Raman data of crystalline $LiNbO_3$. The analysis presented here considers the assignment of the transverse optical (TO) Raman active phonons, and allowed to address still open questions, such as the assignment of the fundamental transitions associated to TO phonons 2 E and 9 E.[2,6–10] Full periodic boundary conditions electronic structure DFT calculations were used, following the LCAO approach as implemented in the CRYSTAL code,[11,12] in order to reproduce the polarized-light Raman pattern associated with the excitation of the TO modes in the limit of static exciting field. As shown below, the obtained results highlight the suitability of the theoretical approach used for the investigation of the structure and phonons properties of the $LiNbO_3$ crystal, as a benchmark test for the application of the method to crystalline materials.

2 | MATERIAL AND METHODS

2.1 | Computational approaches

The full optimization of the *R*3*c* crystal structure of $LiNbO_3$ and the calculation of its Raman spectra have been carried out with the CRYSTAL software package, in the DFT framework,[11,12] using the B3LYP functional[13] and the pob-TZVP basis set.[14–16] For all calculations, the atomic positions and the lattice parameters were optimized. The input structure for the calculations was that experimentally determined by Abrahams et al.[17] The calculations of the vibrational wavenumbers were performed for the optimized geometries using the same method and basis set.

The CRYSTAL code has been used in the past to simulate the properties of other systems similar to $LiNbO_3$[18] and presents relevant advantages for the simulations of polarized Raman spectra. Indeed, by using a Gaussian basis set in the LCAO description of crystal orbitals, hybrid exchange–correlation functionals can be managed much easier than in plane waves codes, thus allowing a more accurate prediction of vibrational spectra. Vibrational wavenumbers were computed by the diagonalization of the dynamical matrix at the Γ point of the first Brillouin zone (BZ) and the Cartesian force constants (i.e., the elements of the Hessian of the potential energy, expressed in mass-weighted atomic Cartesian coordinates) were computed by numerical evaluation of the first derivatives of the analytical atomic gradients.

In CRYSTAL, Raman and infrared (IR) intensities can be predicted accurately through the Coupled Perturbed Kohn Sham (CPKS) method.[11,12] Based on the different components of the Raman tensor, computed as second derivatives of the energy with respect to the electric field, intensities can be calculated and, then, used to predict polarized Raman spectra. The Raman activity of the k normal mode, A_{ij}^k, corresponding to incident and scattered beams with i and j polarization direction, respectively, is computed as $A_{ij}^k = \left(\alpha_{ij}^k\right)^2$, where α_{ij}^k is the i,j component of the Raman tensor associated to mode k. In the limit of static exciting field ($\lambda_{exc} \rightarrow \infty$), Raman intensities I_{ij}^k can then be computed as $I_{ij}^k = \frac{A_{ij}^k}{\omega_k}$, where ω_k is the vibrational wavenumber of the normal mode k.

Indeed, by using a Gaussian basis set in the LCAO description of crystal orbitals, Fock exchange can be computed at a much lower cost with respect to standard plane waves codes,[11,19] allowing to use hybrid exchange–correlation functionals and obtaining a more accurate prediction of vibrational spectra. The wavenumbers computed at this level of theory showed indeed a better agreement with experimental data with respect to plane wave codes (employing local-density approximation or generalized gradient approximation functionals) in different cases.[20–23]

The correspondence between the different components of the CRYSTAL calculated polarized Raman spectra and the experimental spectra obtained using the back-scattering mode in a Horiba LabRam HR Evolution Raman spectrometer, was established as described below.

2.2 | Experimental spectra collection

The $LiNbO_3$ crystal samples (X cut, Y cut, and Z cut; $10 \times 10 \times 0.5$ mm) were bought from PI-KEM, Ltd. X cut, Y cut, and Z cut mean that the crystal face cut is perpendicular to the x, y, and z directions of the crystal, respectively, with z being the polar axis, that is, the direction of the crystal dipole.

The single crystal Raman spectra were obtained in the 50–1000 cm^{-1} Raman shift range, with accuracy better than 0.5 cm^{-1}, using a micro-Raman Horiba LabRam HR Evolution system. The excitation was provided by a solid-state laser at $\lambda = 532$ nm (horizontally polarized; laser power ~50 mW at the sample). In order to collect the polarized spectra, a half-wave polarization rotator (Horiba–Jobin–Yvon) was used to change the polarization of the incident light by 90° and a CorePol P-500-1000 polarizer (Horiba–Jobin–Yvon) was used to select the component of the scattered light to collect. The collection time varied between 2 and 20 s, with 100 accumulations being averaged to produce the final spectra. A 50X objective lens was used, the laser spot diameter being 1 μm at the sample. The wavenumber calibration was performed using the characteristic Si wafer band at 520.5 cm^{-1}.

3 | GENERAL CONCEPTS AND AN OVERVIEW OF PREVIOUS STUDIES ON THE RAMAN SPECTRUM OF $LINBO_3$

The classical theory of Raman scattering is based on the concept that the light scattered by a molecule is generated by oscillating electric dipoles induced by the electric field of the incident (exciting) light beam.[24] The relation between the induced dipole moment vector, $\boldsymbol{\mu}'$, and the external electric field vector, $\boldsymbol{E}$, can be written in a simplified way (ignoring nonlinear terms in the expansion)[24] as follows:

$$\boldsymbol{\mu}' = \bar{\bar{\boldsymbol{\alpha}}}\boldsymbol{E}, \tag{1}$$

where $\bar{\bar{\boldsymbol{\alpha}}}$ is the molecular polarizability tensor.

In the double harmonic approximation,[24] the dipole component responsible for the kth Raman line can be expressed as follows:

$$\boldsymbol{\mu}'_k = \bar{\bar{\boldsymbol{\alpha}}}'_k \boldsymbol{E}\, Q_k, \tag{2}$$

namely,

$$\begin{bmatrix}\mu_x\\ \mu_y\\ \mu_z\end{bmatrix}_k = \begin{bmatrix}\alpha'_{xx} & \alpha'_{xy} & \alpha'_{xz}\\ \alpha'_{yx} & \alpha'_{yy} & \alpha'_{yz}\\ \alpha'_{zx} & \alpha'_{zy} & \alpha'_{zz}\end{bmatrix}_k \begin{bmatrix}E_x\\ E_y\\ E_z\end{bmatrix} Q_k, \tag{3}$$

where the coefficients α'_{ij} correspond to the components of the Raman polarizability tensor $\bar{\bar{\boldsymbol{\alpha}}}'_k$, which contains the first derivatives of $\bar{\bar{\boldsymbol{\alpha}}}$ with respect to a Raman active normal mode Q_k evaluated at the equilibrium geometry of the molecule. In the case of nonresonant Raman scattering, $\bar{\bar{\boldsymbol{\alpha}}}'$ can be described by a real, symmetric matrix where $\alpha'_{ij} = \alpha'_{ji}$ and, therefore, it has, at maximum, six independent components.

In the case of a crystal, the Raman polarizability tensor is commonly referred to the matter belonging to the unit cell.

The contribution of the Raman polarizability tensor to the Raman scattering intensity of the kth normal mode is determined by $\left|\boldsymbol{e_i}\bar{\bar{\boldsymbol{\alpha}}}'_k\boldsymbol{e_s}\right|^2$, where $\boldsymbol{e_i}$ and $\boldsymbol{e_s}$ represent, respectively, the polarizations of the incident and scattered photons.[25] The shape of the Raman tensor $\bar{\bar{\boldsymbol{\alpha}}}'_k$ depends on the symmetry of the kth vibrational mode according to the point group of the molecule or of the crystal, so that the knowledge of the symmetry species to which a given vibrational normal mode belongs allows determining null tensor components and the possible existence of components with identical (or opposite) values.

In the case of a macroscopically oriented sample, $\left|\boldsymbol{e_i}\bar{\bar{\boldsymbol{\alpha}}}'_k\boldsymbol{e_s}\right|^2$ might be equal to 0 for a given specific combination of photon polarizations: in this case, the vibrational mode k is not Raman active for that particular scattering configuration. Hence, by analyzing the shape of the Raman tensor $\bar{\bar{\boldsymbol{\alpha}}}'_k$, it is possible to obtain Raman selection rules for the vibrational modes in different scattering geometries.[26] On the other hand, by careful controlling the polarization of both the incident and scattered photons, the selection rules experimentally determined allow identifying the symmetry of the vibrational modes, thus facilitating vibrational assignments.[26]

It is worth mentioning that also for isotropic samples (e.g., molecules in solution) Raman measurements with polarized light allow to distinguish between totally symmetric and non-totally symmetric modes. Playing with two different experimental setups, where $\boldsymbol{e_i}$ and $\boldsymbol{e_s}$ are parallel (parallel–parallel polarization) or orthogonal (parallel-perpendicular polarization), Raman dichroic ratios can be obtained, which immediately sort polarized totally symmetric transitions from unpolarized ones.

When samples showing orientation of the matter (like, e.g., single crystals) are investigated, the orientation of the sample in the laboratory frame, together with the polarization directions selected for the incident and scattered light beams, makes it possible to determine—from different complementary Raman experiments—the components of the Raman tensor. In particular, from *relative* bands intensities of judiciously chosen polarized Raman spectra one can extract information on the *relative* values of the relevant polarizability components for the different Raman active modes. On the other hand, thanks to the current accuracy of the state-of-the-art computational approaches to predict Raman intensities, by exploiting the synergic use of theory and experiments the individual polarizability components can be determined. Furthermore, the evaluation of the quality of the computed Raman spectral patterns mimicking experiments performed with polarized light allows to assess the performance of the used theoretical approach to describe the individual elements of the Raman tensors, thus providing a sound validation of the theoretical Raman activities obtained by calculations.

The $\Gamma = 0$ phonons of the room temperature phase (*R*3*c*) crystal of $LiNbO_3$ are classified in the irreducible representation as $4A_1$, $5A_2$, and 9E, where the A_1 (polarized along *Z*) and the E (polarized in the *XY* plane) modes are Raman active, whereas the A_2 modes are silent.[2,6] By choosing the reference Cartesian *XYZ* system in such a way that *Z* is aligned along the polar axis of the $LiNbO_3$ crystal and *X* is aligned along the crystallographic axis *a*, the Raman polarizability tensors of the E and A_1 modes show the following general form[27]:

$$A_1(Z) = \begin{pmatrix} a & 0 & 0 \\ 0 & a & 0 \\ 0 & 0 & b \end{pmatrix}, \quad E(X) = \begin{pmatrix} c & 0 & d \\ 0 & -c & 0 \\ d & 0 & 0 \end{pmatrix}, \quad E(Y) = \begin{pmatrix} 0 & -c & 0 \\ -c & 0 & d \\ 0 & d & 0 \end{pmatrix}, \tag{4}$$

where *a*, *b*, *c*, −*c*, and *d* represent non-null Raman polarizability tensors component values.

Each phonon at $\Gamma = 0$ gives rise to a pair of observable Raman transitions at different wavenumbers, corresponding to longitudinal optical (LO) and transverse optical (TO) phonons.[7,25] As discussed by Parlinski and Li,[10] calculation of the forces at $\Gamma = 0$ according to the direct method allows to predict the wavenumbers corresponding to TO phonons, while a reliable calculation of LO phonon wavenumbers requires that explicit consideration of the interactions with the macroscopic electric field generated by lattice polar vibrations and are not accessible by direct method calculations.

Vibrational assignments for $LiNbO_3$ crystal have already been proposed in the literature, both experimentally and theoretically.[2,6,8–10,28–33] Table 1 shows the experimentally measured Raman wavenumbers and the vibrational assignment of TO e LO phonons of $LiNbO_3$ according to the recent review by Fontana and Bourson.[8] Note that the 2 E and 9 E modes (see Table 1—in bold) have been assigned differently in the literature.[2,6–10,28–33] As described below, the present study will add evidence for settling this point.

Fontana and Bourson[8] reported also the expected modes that could be seen in polarized Raman spectra of an oriented single crystal of $LiNbO_3$, exploiting different experimental polarization setups, which are summarized

TABLE 1 Experimental wavenumbers of the $LiNbO_3$ vibrational modes (A_1 and E symmetries) and their assignment, according to Fontana and Bourson[8]

Vibrational mode	Wavenumber/cm^{-1} TO	LO	Assignment (motions)
1 A_1	254	272	$Nb_{(z)}$, $O_{(z)}$
2 A_1	275	332	$Nb_{(z)}$, $Li_{(z)}$
3 A_1	332	419	$O_{(x,y)}$
4 A_1	631	871	$O_{(x,y)}$
1 E	152	186	$Nb_{(x,y)}$, $O_{(x,y)}$
2 E	**186**	194	*all atoms*$_{(all\ directions)}$
3 E	236	238	
4 E	263	295	
5 E	322	366	
6 E	369	425	
7 E	432	456	
8 E	578	625	
9 E	**738**	880	$Nb_{(x,y)}$, $O_{(x,y,z)}$

Note: The assignments for the 2 E and 9 E modes (wavenumbers highlighted in bold) have been debated.
Abbreviations: LO, longitudinal optical; TO, transverse optical.

for the back-scattering geometry in Table 2. In this table, the Porto notation is used to describe the geometry adopted in the polarized Raman experiments. According to this notation, a set of four symbols is used, $K_1(P_1,P_2)K_2$, where K_1 and K_2 are the directions of the incident and scattered waves (for the back-scattering collection mode, K_2 is equal to $\bar{K}_1$, where the trace over the letter means opposite direction), while P_1 and P_2 denote the direction of the polarization of each wave.

TABLE 2 Phonon modes expected to be visible in the different polarized Raman spectra of $LiNbO_3$, for back-scattering mode, and their respective experimental wavenumbers according to Fontana and Bourson[8]

Experimental configuration (Porto notation)	Expected visible modes	Wavenumber/cm^{-1}
$X(YY)\bar{X}$	A_1 (TO) + E (TO)	152, 186, 236, 254, 263, 275, 322, 332, 369, 432, 578, 631, and 738
$X\,(YZ)\bar{X}$	E (TO)	152, 186, 236, 263, 322, 369, 432, 578, and 738
$X\,(ZY)\bar{X}$	E (TO)	152, 186, 236, 263, 322, 369, 432, 578, and 738
$X\,(ZZ)\bar{X}$	A_1 (TO)	254, 275, 332, and 631
$Y\,(XX)\bar{Y}$	A_1 (TO) + E (LO)	186, 194, 238, 254, 275, 295, 332, 366, 425, 456, 625, 631, and 880
$Y\,(XZ)\bar{Y}$	E (TO)	152, 186, 236, 263, 322, 369, 432, 578, and 738
$Y\,(ZX)\bar{Y}$	E (TO)	152, 186, 236, 263, 322, 369, 432, 578, and 738
$Y\,(ZZ)\bar{Y}$	A_1 (TO)	254, 275, 332, and 631
$Z\,(YX)\bar{Z}$	E (TO)	152, 186, 236, 263, 322, 369, 432, 578, and 738
$Z\,(XY)\bar{Z}$	E (TO)	152, 186, 236, 263, 322, 369, 432, 578, and 738
$Z\,(XX)\bar{Z}$	A_1 (LO) + E (TO)	152, 186, 236, 263, 272, 322, 332, 369, 419, 432, 578, 738, and 871
$Z\,(YY)\bar{Z}$	A_1 (LO) + E (TO)	152, 186, 236, 263, 272, 322, 332, 369, 419, 432, 578, 738, and 871

In the theoretical work by Parlinski and Li,[10] phonon dispersion curves for $LiNbO_3$ were obtained in the framework of DFT, according to the local-density approximation with ultrasoft pseudopotentials and a plane wave basis set, and the LO and TO phonon wavenumbers for the Raman active transitions were reported. Using the same theoretical framework, Hermet et al.[2] predicted the polarized Raman spectra of $LiNbO_3$ (wavenumbers and intensities) by calculating the derivatives of the linear optical susceptibility with respect to atomic displacements (using a first-principles approach based on DFT and taking advantage of an implementation based on the nonlinear response formalism and the $2n + 1$ theorem). In turn, Caciuc and Postnikov[9] reported accurate TO Γ phonon wavenumbers from first-principles calculations using the full-potential linearized augmented plane waves method within the frozen phonon approximation.

In the present work, the TO phonon wavenumbers and Raman activities have been calculated at $\Gamma = 0$, and a comparison between the experimental wavenumbers determined in this work and those reported by Fontana and Bourson[8] will be presented in the next section. The theoretically obtained wavenumbers will be compared with the results reported by Caciuc and Postnikov,[9] and with the experimentally obtained data. Finally, the intensity patterns (relative intensities of the bands) predicted for selected experimental polarization setups and its correlation with the experimental data will be discussed in detail.

4 | RESULTS AND DISCUSSION

In the present study, the Raman spectra have been obtained using three different crystal orientations with respect to the laser beam direction, namely, at incidence normal to the three cut surfaces of the crystal, identified by their normal vector as *X* cut, *Y* cut, and *Z* cut. For each crystal orientation, four different combination of polarization of the incident and scattered radiation were selected, thus providing a total number of 12 experimental spectra. Figure 1 presents the geometric configurations determining the polarization of the laser beam relatively to the sample in the used instrument (Horiba LabRam HR evolution).

Table 3 provides the equivalence of the used geometries to the experimental configurations according to Porto notation. As shown in the table, $X(YY)\bar{X}$, $X\,(YZ)\bar{X}$, $X(ZY)\bar{X}$, and $X(ZZ)\bar{X}$ correspond to the *X* cut collection with the incident-scattered light polarizations horizontal–horizontal, horizontal–vertical, vertical–horizontal, and vertical–vertical, respectively, while the *Y* cut slide spectra collected with the incident–scattered

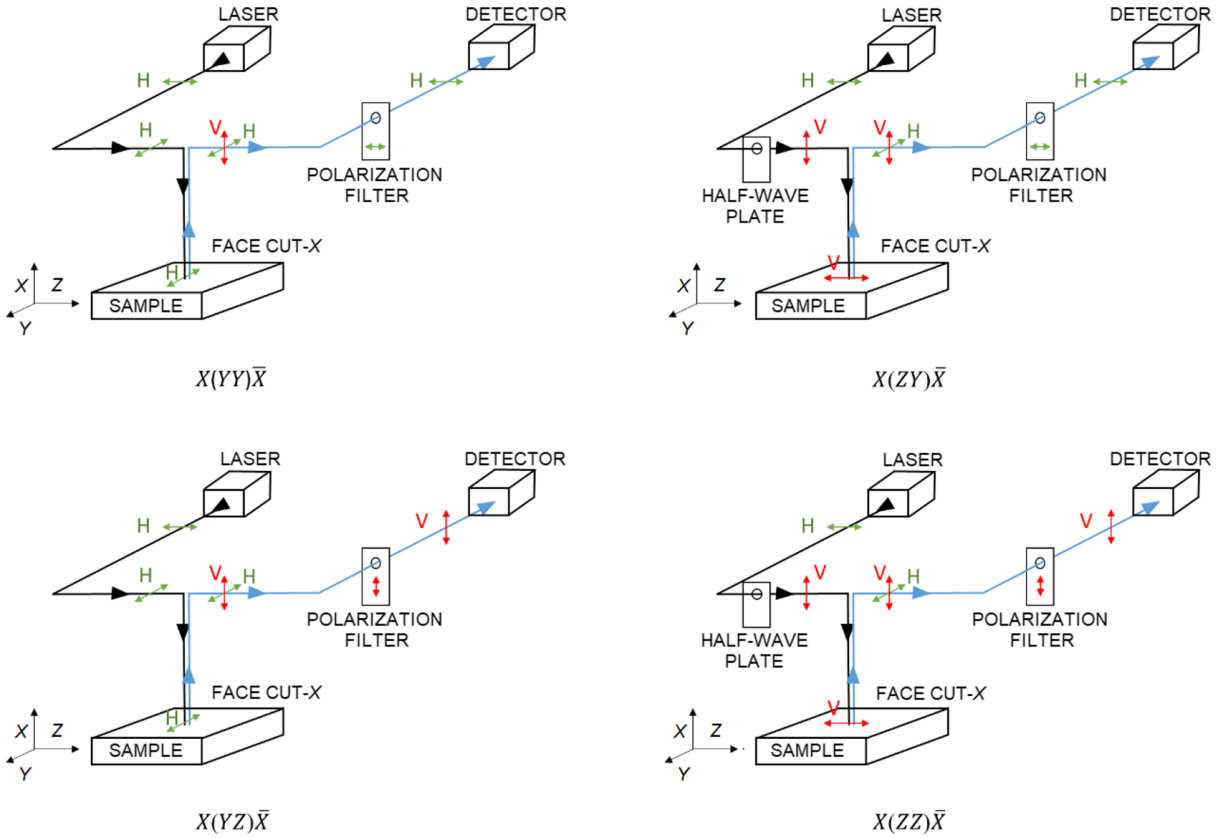

FIGURE 1 Schematic representation of the geometric configurations determining the polarization of the laser beam relatively to the sample in the used instrument (Horiba LabRam HR evolution). The black and blue traces correspond to the incident and scattered beams, respectively. The double arrows represent the direction of the polarization of the beam, classified as horizontal (H) and vertical (V) in the reference frame of the laboratory. The depicted Cartesian vectors, *X*, *Y*, and *Z*, refer to the crystal sample reference frame and vary for the different crystal cuts. The shown examples correspond to the four different configurations for the crystal cut *X* (the corresponding Porto notations are also given). The lithium niobate structure in this crystal cut *X* configuration, is presented in Figure S1 [Colour figure can be viewed at wileyonlinelibrary.com]

TABLE 3 Correspondence between experimental configurations according to Porto notation and the used experimental set ups

	Horiba LabRam HR evolution experimental configurations		
Porto notation	**Crystal cut**	**Incident light polarization**	**Scattered light polarization**
$X\,(YY)\bar{X}$	*X* cut	Horizontal	Horizontal
$X\,(YZ)\bar{X}$		Horizontal	Vertical
$X\,(ZY)\bar{X}$		Vertical	Horizontal
$X\,(ZZ)\bar{X}$		Vertical	Vertical
$Y\,(XX)\bar{Y}$	*Y* cut	Horizontal	Horizontal
$Y\,(XZ)\bar{Y}$		Horizontal	Vertical
$Y\,(ZX)\bar{Y}$		Vertical	Horizontal
$Y\,(ZZ)\bar{Y}$		Vertical	Vertical
$Z\,(XY)\bar{Z}$	*Z* cut	Horizontal	Vertical
$Z\,(YX)\bar{Z}$		Vertical	Horizontal
$Z\,(XX)\bar{Z}$		Horizontal	Horizontal
$Z\,(YY)\bar{Z}$		Vertical	Vertical

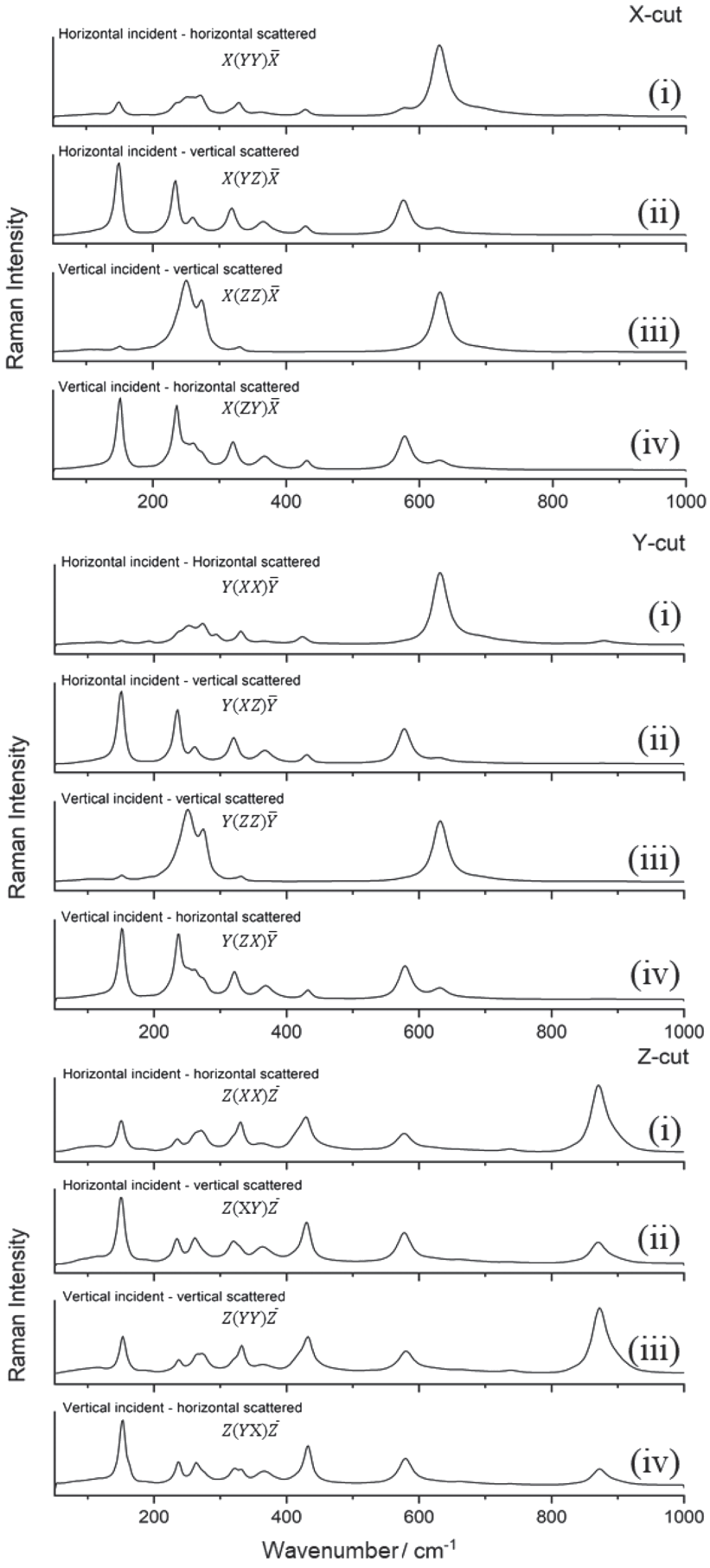

FIGURE 2 Experimental polarized Raman spectra of $LiNbO_3$ crystal (*X* cut: top; *Y* cut: middle; and *Z* cut: bottom) collected for the different possible configurations in the back-scattering mode

polarizations horizontal–horizontal, horizontal–vertical, vertical–horizontal, and vertical–vertical correspond to $Y(XX)\bar{Y}$, $Y(XZ)\bar{Y}$, $Y(ZX)\bar{Y}$, and $Y(ZZ)\bar{Y}$ Porto notations, respectively. In the Z cut analysis, $Z(XY)\bar{Z}$ and $Z(YX)\bar{Z}$ correspond to horizontally–vertically and vertically–horizontally polarized waves and $Z(XX)\bar{Z}$ and $Z(YY)\bar{Z}$ to horizontally–horizontally and vertically–vertically polarized light experiments, respectively.

The experimental spectra of the studied $LiNbO_3$ crystal, collected for all possible back-scattering configurations, are presented in Figure 2. Because of the crystal symmetry at Γ, in the absence of any external electric field the set of spectra corresponding to X and Y cuts should be superimposable. However, in presence of a macroscopic electric field the degeneracy of E modes is removed,[7,10] giving rise to different spectra in correspondence to the X $(YY)X$ set up (A_1(TO) + E (TO)) and Y $(XX)Y$ set up (A_1(TO) + E (LO)). As expected, geometries related by simple exchange of X and Y indexes in the Porto notation give superimposable spectra in all the other cases, namely, all four spectra corresponding to X cut and Y cut spectra (ii) and (iv) in Figure 2 practically coincide; spectra (iii) in these two crystal cut orientations do also coincide; and the Z cut setup provides only two different spectra, corresponding to the pairs (i)/(iii) and (ii)/(iv). These results provide evidence that good control of the experimental set up (crystal orientation and light polarization) was achieved in the performed experiments.

Figure 3 shows the calculated $LiNbO_3$ spectrum constructed taking into account the whole Raman tensor (spectrum [v] in the figure, mimicking an isotropic distribution of $LiNbO_3$ crystals), and the spectra built using the individual components of the Raman tensor (spectra [i] to [iv] in the figure). As already mentioned, according to the capabilities of the used theoretical approach in all the calculated spectra only the TO modes are considered.

4.1 | Wavenumbers

Figure 4 allows to compare the spectra collected in the X $(ZZ)\bar{X}$ and $Y(ZZ)\bar{Y}$ experimental set ups (which probe only A_1 phonons) with that of the calculated spectrum obtained using the α'_{zz} component of the Raman tensors (the b values in Equation 4). The wavenumbers are collected in Table 4. As it can be seen by comparing both the spectral patterns and wavenumbers, the agreement between our experimental and calculated results is remarkable. The appearance of a small peak in the experimental spectra at 152 cm^{-1}, which is not predicted by the calculations, is an evidence of the excitation of a phonon of E species, which should be not allowed by symmetry in this configuration (see Table 3). Its presence in the experimental spectrum might be ascribed to some crystal misalignment, or, more probably, to the actual efficiency of the polarizer that might have not completely filtered the scattered light with horizontal polarization. Indeed, the $X(ZY)\bar{X}$ and $Y(ZX)\bar{Y}$ spectra both show E (TO) transitions, among which 1 E at 152 cm^{-1} is the most intense one (see Figure 5 and Table 5). The A_1 phonons experimental wavenumbers we have measured are

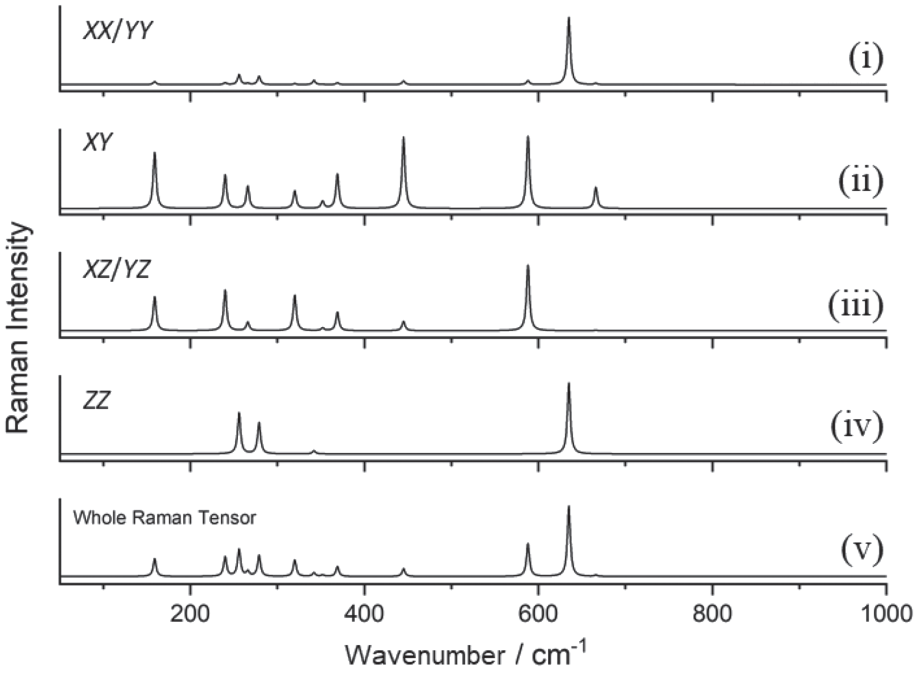

FIGURE 3 CRYSTAL B3LYP/pob-TZVP calculated spectra of the $LiNbO_3$ crystal, considering the whole and individual components of the Raman tensors (abbreviated in the figure using only their Cartesian indexes). All spectra are normalized by their highest intensity peak

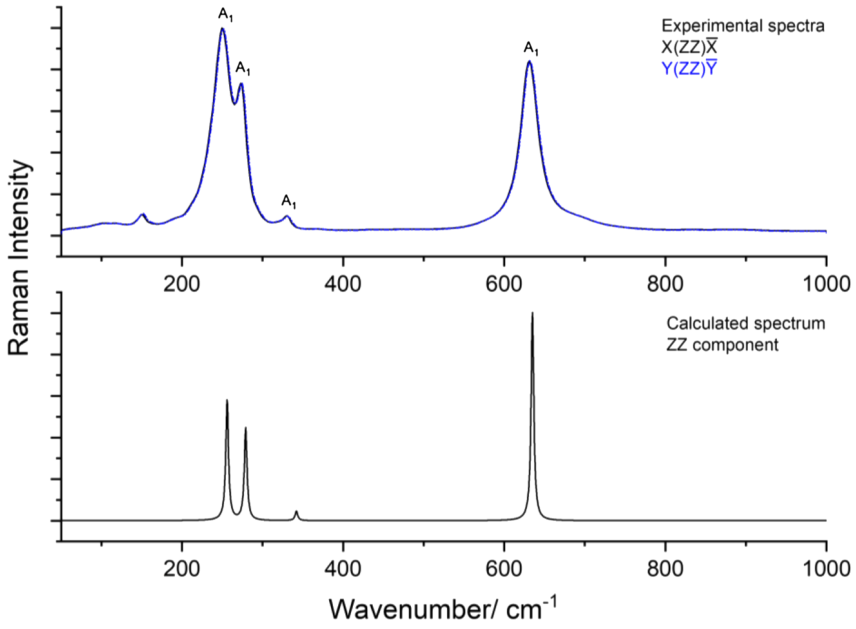

FIGURE 4 Top panel: experimental $X(ZZ)\bar{X}$ (black) and $Y(ZZ)\bar{Y}$ (blue) spectra of $LiNbO_3$ crystal. Bottom panel: CRYSTAL B3LYP/pob-TZVP calculated spectrum based on the α'_{zz} Raman tensors component values [Colour figure can be viewed at wileyonlinelibrary.com]

TABLE 4 Wavenumbers (cm^{-1}) of the phonons observed in the $X(ZZ)\bar{X}/Y(ZZ)\bar{Y}$ experimental spectra of $LiNbO_3$ crystal, CRYSTAL B3LYP/pob-TZVP calculated wavenumbers with non-null intensities according to the α'_{zz} Raman tensors component, and comparison with literature data

Experimental (this work)[a]	Fontana and Bourson[8]	Calculated (this work)	Caciuc et al.[9]	Assignment
252	254	256	208	1 A_1 (TO)
274	275	280	279	2 A_1 (TO)
331	332	342	344	3 A_1 (TO)
632	631	635	583	4 A_1 (TO)

[a]An additional minor band was observed in the experimental spectra, at 152 cm^{-1}, which is ascribable to the 1 E vibration (see text).

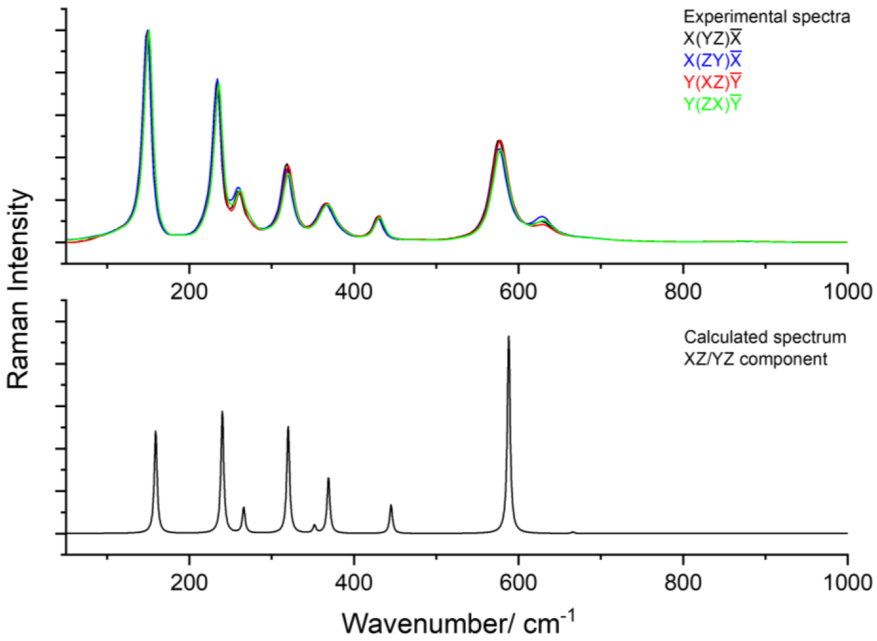

FIGURE 5 Top panel: experimental $X(YZ)\bar{X}$ (black), $X(ZY)\bar{X}$ (blue), $Y(XZ)\bar{Y}$ (red), and $Y(ZX)\bar{Y}$ (green) spectra of $LiNbO_3$ crystal. Bottom panel: CRYSTAL B3LYP/pob-TZVP calculated spectrum based on the α'_{xz} and α'_{yz} components of the Raman tensors [Colour figure can be viewed at wileyonlinelibrary.com]

in very good agreement with the data reported in the work by Fontana and Bourson.[8] Moreover, it is also clear that the wavenumbers prediction by the present calculations—showing errors not exceeding 3%—is much more accurate than that reported previously by Caciuc and Postnikov[9] (errors between 1% and 17%), who also focused on the prediction on the TO vibrations.

The experimental spectra collected in the $X(YZ)\bar{X}$, $X(ZY)\bar{X}$, $Y(XZ)\bar{Y}$, and $Y(ZX)\bar{Y}$ arrangements are compared in Figure 5 with the theoretical spectrum displaying intensities computed using the α'_{xz} and α'_{yz} components of E(X) and E(Y) Raman tensors, respectively, which are identical because of symmetry (d values in Equation 4). The experimental spectra showing deconvolution of the individual bands are presented in Figure S2. The agreement between the experimental and calculated data is noteworthy, with all experimentally observed bands being well predicted by the calculations both regarding wavenumber and intensity. The attained accuracy in the wavenumbers improves on those of previous works.[9] The calculated bands at 352 and 369 cm^{-1} merge into a single broad band at 366 cm^{-1} in the experimental spectra, which after deconvolution reveals two components at 359 and 369 cm^{-1} (see Figure S2), also in good agreement with the calculated values.

It is important to underline that only seven among the nine E symmetry TO modes assigned to fundamental transitions in the last published experimental work on $LiNbO_3$[8] can be reasonably correlated to the present predicted values (see Table 5). Indeed, the previously reported very weak feature at 186 cm^{-1} does not find any correspondence with our predicted Raman transitions. This band has been assigned before[8] to both TO and LO E phonons, and the present results strongly suggest that it is only due to the LO mode. Considering also the fact that the feature observed at 366 cm^{-1} corresponds, as already mentioned above, to the two E (TO) modes predicted at 352 and 369 cm^{-1}, a reassignment of the lowest wavenumbers E (TO) modes is proposed here that fits all these evidences (see Table 5). Moreover, we propose also to reassign the 9 E phonon to the feature observed at 670 cm^{-1}, which fits both our prediction (666 cm^{-1}) and that of Cauciuc and Postnikov[9] (617 cm^{-1}) better than the weaker feature observed at 738 cm^{-1} by Fontana and Bourson[8] and that could not be observed in our spectra.

Note also that, as above, the present experimental spectra also show one weak extra band (632 cm^{-1}), which shall be ascribed to an A_1 mode (strictly not allowed by symmetry in these experimental configurations). This band is the most intense band in the $X(YY)\bar{X}$ spectrum (see Figure 6) and partially overlap the 9 E band, which is, however, clearly visible in the deconvoluted spectrum shown in Figure S2.

The patterns of the $X(YY)\bar{X}$ Raman and $Y(XX)\bar{Y}$ spectra are quite complex, because of the simultaneous presence of A_1 (TO) and E (TO) or A_1 (TO) and E (LO) transitions, respectively. The spectra are determined by the α'_{yy} and α'_{xx} components of the Raman tensors (a and $c/-c$ values in Equation 4 for A_1 and E modes, respectively). The results are shown in Figure 6 and Table 6 (and also in Figure S3, which presents the bands deconvolution results). In the case of the $Y(XX)\bar{Y}$

TABLE 5 Wavenumbers (cm^{-1}) of the phonons observed in the $X(YZ)\bar{X}/X(ZY)\bar{X}/Y(XZ)\bar{Y}/Y(ZX)\bar{Y}$ experimental spectra of $LiNbO_3$ crystal, CRYSTAL B3LYP/pob-TZVP calculated wavenumbers with non-null intensities according to the α'_{xz} and α'_{yz} Raman tensors components, and comparison with literature data

Experimental (this work)[a]	Fontana and Bourson[8][b]	Calculated (this work)	Caciuc et al.[9]	Assignment[c]
152	152	159	151	1 E (TO)
237	236	240	167	2 E (TO)
261	263	266	236	3 E (TO)
320	322	320	307	4 E (TO)
359	-	352	334	5 E (TO)
369	369	369	352	6 E (TO)
432	432	445	432	7 E (TO)
579	578	588	526	8 E (TO)
670	738	666	617	9 E (TO)

[a]An additional minor band was observed in the experimental spectra, at 632 cm^{-1}, which is ascribable to the 4 A_1 vibration (see text); wavenumbers in italic correspond to the bands for whom reassignment is proposed.

[b]In Fontana and Bourson,[8] the 2 E mode has been assigned to a very weak band at 186 cm^{-1} (also ascribed to a E (LO) mode), so that the next 4 observed E bands were assigned to 3 E, 4 E, and 5 E (see discussion in the text).

[c]The numbering of the vibrations follows an increasing order of the wavenumbers and strictly applies only to our own assignment.

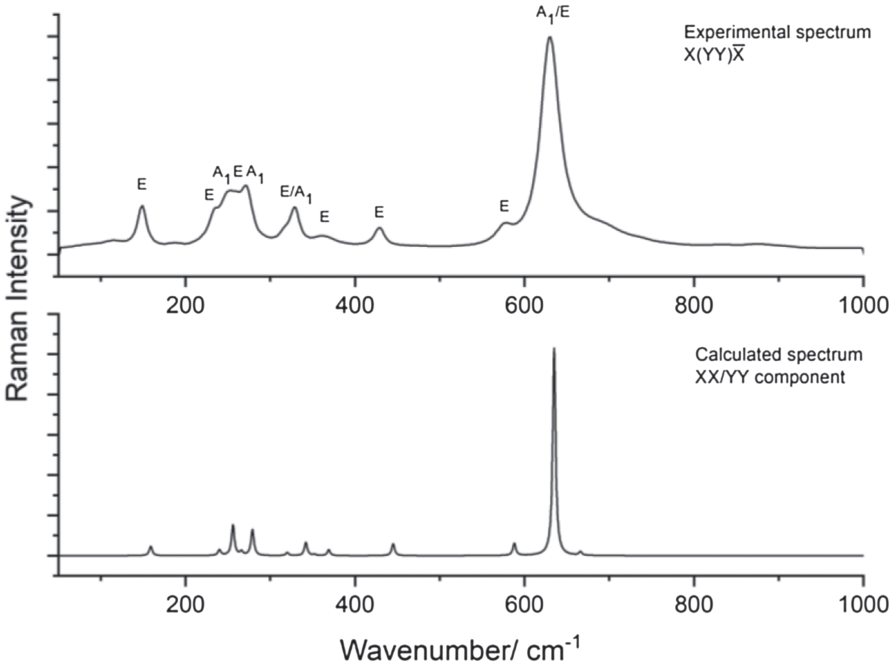

FIGURE 6 Top and middle panels: experimental $X(YY)\bar{X}$ and $Y(XX)\bar{Y}$ spectra of $LiNbO_3$ crystal, respectively. Bottom panel: CRYSTAL B3LYP/pob-TZVP calculated spectrum based on the α'_{xx} and α'_{yy} components of the Raman tensors

spectrum, the present experimental results generally agree with those reported previously (see Table 6).[8,29,30,33] Our calculations do not provide wavenumber values for the E (LO) modes, but the calculated data for the A_1 phonons fit nicely the experimental results. The results of the calculations by Parlinski and Li[10] regarding the wavenumbers of the E (LO) modes are shown in Table 6, but one can see that the general agreement of the calculated values with the experimental data is modest.

The results for the case of the $X(YY)\bar{X}$ arrangement are particularly interesting, because all transitions of TO type (both of A_1 and E symmetries) are expected to contribute to the Raman spectrum, so that the data allow a more general comparison between the calculated and experimental results than when each set of bands (A_1 or E) is considered in separate (as in Figures 4 and 5). It can be seen that the general agreement between the experimental and calculated data obtained in the present investigation is remarkable, independently of the symmetry of the vibrations. In the $X(YY)\bar{X}$ experimental spectrum, the two pairs of bands predicted at 320/342 and 352/369 cm^{-1} appear as two broad bands with maxima at 329 and 361 cm^{-1}, respectively. These bands could be successfully deconvoluted (see Figure S3), resulting in components with maxima at 320/331 and 359/369 cm^{-1}, respectively, which are in good agreement with the theoretically predicted values.

Figure 7 presents the comparison of the Raman spectra obtained using the pairs $Z(XX)\bar{Z}/Z(YY)\bar{Z}$ and $Z(XY)\bar{Z}/Z(YX)\bar{Z}$ of experimental configurations, together with the predicted spectrum built using the α'_{xy} component of the Raman tensors for the E modes ($-c$ value, Equation 4). Band deconvolution of the experimental bands is presented in Figure S4. According to Table 2, both A_1 (LO) and E (TO) modes should be seen in the first pair of configurations, while only the E (TO) modes should be observed in the second one. All E (TO) vibrations are observed in the two pairs of experimental configurations, as expected. The A_1 (LO) modes are observed at 273, 331, 412, and 872 cm^{-1}, in good agreement with previous data (see Table 7).[8] The calculated wavenumbers reported by Parlinski and Li[10] for these modes are also included in Table 7, showing a relatively modest agreement with the experimental values. In the case of the $Z(XY)\bar{Z}/Z(YX)\bar{Z}$, besides the expected bands due to E (TO) vibrations, a band ascribable to residual intensity of the most intense LO A_1 mode at 872 cm^{-1} (observed in the $Z(XX)\bar{Z}$ and $Z(YY)\bar{Z}$ configurations) is also observed, most probably due to a minor crystal misalignment or incomplete filtering of the scattered light.

4.2 | Intensities

In this section, the comparison between the Raman intensity patterns of the calculated and experimental spectra is presented. The data are summarized in Tables 8–11: Table 8 for the A_1 (TO) modes (comparison between the calculated spectrum based on the α'_{zz} Raman tensor components and the $\boldsymbol{X(ZZ)\bar{X}}/Y(ZZ)\bar{Y}$ experimental configuration spectra; the first experimental

TABLE 6 Wavenumbers (cm^{-1}) of the phonons observed in the experimental $X(YY)\bar{X}$ and $Y(XX)\bar{Y}$ spectra of $LiNbO_3$ crystal, CRYSTAL B3LYP/pob-TZVP calculated wavenumbers with non-null intensities according to the α'_{xx} and α'_{yx} Raman tensors components, and comparison with literature data

Experimental (this work)		Fontana and Bourson[8]a				
X **$(YY)\bar{X}$**	***Y*** **$(XX)\bar{Y}$**	***X*** **$(YY)\bar{X}$**	***Y*** **$(XX)\bar{Y}$**	**Calculated (this work)**	**Caciuc et al.[9] and Parlinski and Li[10]b**	**Assignment[c]**
152		152		159	151	1 E (TO)
	150		186	-	204	1 E (LO)
	191		194	-	216	2 E (LO)
237		236		240	167	2 E (TO)
	237		238	-	316	3 E (LO)
252	252	254	254	256	208	1 A_1 (TO)
261		263		266	236	3 E (TO)
274	274	275	275	280	279	2 A_1 (TO)
	295		295	-	372	4 E (LO)
320		322		320	307	4 E (TO)
331	331	332	332	342	334	3 A_1 (TO)
359		-		352	344	5 E (TO)
	368		366	-	422	5 E (LO)
369		369		369	352	6 E (TO)
	423		425	-	445	6 E (LO)
432		432		445	432	7 E (TO)
	575		456d	-	570	7 E (LO)
579		578		588	526	8 E (TO)
	689		625e	-	677	8 E (LO)
632	632	631	631	635	583	4 A_1 (TO)
670		738		666	617	9 E (TO)
	880		880	-	856	9 E (LO)

[a]In Fontana and Bourson,[8] the 2 E mode has been assigned to a very weak band at 186 cm^{-1} (also ascribed to the 1 E (LO) mode), so that the next 4 observed E bands were assigned to 3 E, 4 E, and 5 E (see discussion in the text).
[b]Caciuc et al.[9] for TO modes and Parlinski and Li[10] for LO modes.
[c]The numbering of the vibrations follows an increasing order of the wavenumbers and strictly applies only to our own assignment.
[d]In Yang et al.,[33] this mode was assigned to a band reported at 530 cm^{-1}.
[e]In Claus and Borstel,[29], this mode was assigned to a band reported at 668 cm^{-1}.

configuration was used for quantitative measurements of intensities), Tables 9 and 10 for the E (TO) modes (comparison between the calculated spectrum based on the α'_{xz} and α'_{yz} components of the Raman tensors and the $\boldsymbol{Y(XZ)\bar{Y}}$, $X(ZY)\bar{X}$, $Y(XZ)\bar{Y}$, and $Y(ZX)\bar{Y}$ experimental spectra and between that calculated based on the α'_{xy} and α'_{yx} components of the Raman tensors and the $\boldsymbol{Z(XY)\bar{Z}}$) and $Z(YX)\bar{Z}$) experimental spectra, respectively, Table 11 for both A_1 (TO) and E (TO) modes (comparison between the calculated spectrum based on the α'_{yy}—equal to α'_{xx}—components of the Raman tensors and the $X(YY)\bar{X}$ experimental spectrum). For the comparison of the relative intensities of the bands, a well-isolated band was chosen as reference in each spectrum (bands ascribable to 3 A_1 and 7 E [TO] modes satisfy this criterion and were then selected) and the intensities of the other bands were compared with that of the reference band. Experimental intensities were obtained by band area determination.

The correspondence between the Raman relative intensities of the experimental spectra and of the spectra calculated in the present study is quite remarkable, strongly improving on previous results[2] where only a very modest agreement was obtained (in the present study, the average error in the calculated relative

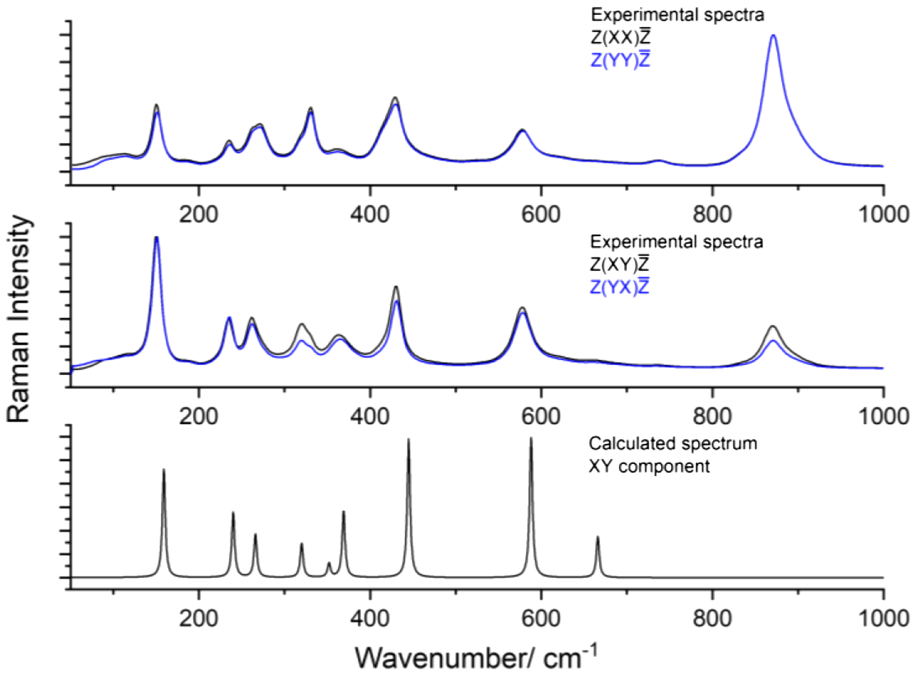

FIGURE 7 Top panel: experimental $Z(XX)\bar{Z}$ (black) and $Z(YY)\bar{Z}$ (blue) spectra of $LiNbO_3$ crystal. Middle: experimental $Z(XY)\bar{Z}$ (black) and $Z(YX)\bar{Z}$ (blue) spectra of $LiNbO_3$ crystal. Bottom panel: CRYSTAL B3LYP/pob-TZVP calculated spectrum based on the α'_{xy} component of the Raman tensors [Colour figure can be viewed at wileyonlinelibrary.com]

TABLE 7 Wavenumbers (cm^{-1}) of the A_1 (LO) phonons observed in the experimental $Z(XX)\bar{Z}$ and $Z(YY)\bar{Z}$ spectra of $LiNbO_3$ crystal and comparison with literature data

Experimental (this work)	Fontana and Bourson[8]	Calculated (Parlinski and Li[10])	Symmetry
273	272	309	1 A_1 (LO)
331	332	381	2 A_1 (LO)
412	419	548	3 A_1 (LO)
872	871	831	4 A_1 (LO)

TABLE 8 Comparison between the Raman intensities (areas under the bands) of the calculated spectrum based on the α'_{zz} Raman tensor components and the $X(ZZ)\bar{X}$ experimental configuration spectrum (A_1 symmetry modes)

		Relative intensity			
Mode	Calculated wavenumber (cm^{-1})	Calculated (a.u.)		Experimental (a.u.)	
1 A_1	256	13.4	*23.4*	16.1	*24.3*
2 A_1	280	10.0		8.2	
3 A_1	**342**	**1**		**1**	
4 A_1	635	22.4		22.2	

Note: The band due to the 3 A_1 mode was chosen as reference (in bold). Intensities in relative arbitrary units (a. u.). Values in italic correspond to sums for bands whose individual intensities resulted from band deconvolution.

intensities, compared to experimental ones, is ~10%, while from the graphical data presented in Hermet et al.[2] an error larger than twice the one obtained in this study can be estimated).

Comparison of the A_1 Raman intensities presented in Table 8 (see also Figure 4) allows to conclude that there is an almost perfect correspondence regarding the experimental and calculated relative intensities for Mode 4 A_1 (22.2 vs. 22.4) regarding the 3 A_1 mode, set as reference, and also a very good agreement between those of Modes 1 A_1 (16.1 vs. 13.4) and 2 A_1 (8.2 vs. 10.0). It must be noticed that for the two later modes, the individual intensities resulted from band deconvolution (which is particularly difficult in this case due to the close proximity of the two maxima) and that the agreement between the total experimental and calculated intensity of this pair of bands is in fact excellent (24.3 vs. 23.4).

An excellent correspondence is also observed in the case of the more complex spectra of the E (TO) modes (see Figures 5 and 7 and Tables 9 and 10). In fact, with

TABLE 9 Comparison between the Raman intensities (areas under the curve) of the calculated spectrum based on the α'_{xz} and α'_{yz} Raman tensor components and the $Y(XZ)\bar{Y}$ experimental configuration spectrum (E symmetry modes)

Mode	Calculated wavenumber (cm^{-1})	Relative intensity			
		Calculated (a.u.)		Experimental (a.u.)	
1 E	159	3.7		3.8	
2 E	240	4.2		3.7	
3 E	266	1.0		1.8	
4 E	320	3.7		3.9	
5 E	352	0.4	2.3	0.3	*2.7*
6 E	369	1.9		2.4	
7 E	**445**	**1**		**1**	
8 E	588	7.0		7.6	
9 E	666	0.1		0.1	

Note: The band due to the 7 E mode was chosen as reference (in bold). Intensities in relative arbitrary units (a. u.). Values in italic correspond to sums for bands whose individual intensities resulted from band deconvolution.

TABLE 10 Comparison between the Raman intensities (area under the curve) of the calculated spectrum based on the α'_{xy} and α'_{yx} components of the Raman tensors and the $Z(XY)\bar{Z}$ experimental configuration spectrum (E symmetry modes)

Mode	Calculated wavenumber (cm^{-1})	Relative intensity			
		Calculated (a.u.)		Experimental (a.u.)	
1 E	159	0.7		0.8	
2 E	240	0.4		0.5	
3 E	266	0.3		0.3	
4 E	320	0.3		0.3	
5 E	352	0.2	*0.5*	0.1	*0.6*
6 E	369	0.3		0.5	
7 E	**445**	**1**		**1**	
8 E	588	1.0		1.0	
9 E	666	0.2		0.3	

Note: The band due to the 7 E mode was chosen as reference (in bold). Intensities in relative arbitrary units (a. u.). Values in italic correspond to sums for bands whose individual intensities resulted from band deconvolution.

TABLE 11 Comparison between the Raman intensities (area under the curve) of the calculated spectrum based on the α'_{yy} component of the Raman tensors and the $X(YY)\bar{X}$ experimental configuration spectrum (A_1 and E symmetry modes)

Mode	Calculated wavenumber (cm^{-1})	Relative intensity			
		Calculated (a.u.)		Experimental (a.u.)	
1 E	159	0.8		0.8	
2 E	240	0.5		0.5	
1 A_1	256	2.2		2.5	
3 E	266	0.4		0.5	
2 A_1	280	1.8		2.2	
4 E	320	0.2	*1.1*	0.2	*1.3*
3 A_1	342	0.9		1.1	
5 E	352	0.2	*0.6*	0.2	*0.7*
6 E	369	0.4		0.5	
7 E	**445**	**1**		**1**	
8 E	588	1.1		1.0	
4 A_1	635	13.7		16.9	
9 E	666	0.5		0.4	

Note: The band due to the 7 E mode was chosen as reference (in bold). Intensities in relative arbitrary units (a. u.). Values in italic correspond to sums for bands whose individual intensities resulted from band deconvolution.

the exception of 3 E mode in the *XZ*/*YZ* spectrum, whose calculated relative intensity is about one half the experimental value, the intensity pattern is remarkably well predicted by the calculations.

Similarly, the intensity pattern of the full set of A_1 and E modes observed in $X(YY)\bar{X}$ experimental spectrum is very well predicted by the *XX*/*YY* calculated spectrum. The biggest difference between the relative intensity of experimental and theoretical spectra appears in the 4 A1 mode. In both cases, this is the clearly the highest peak; see Figure 6 and Table 11, meaning that the difference in the relative intensity of this particular vibration is not significant to alter the structure of the spectra, which is in fact very similar. Therefore, our calculations predict well both A_1 and E modes intensity when they appear in simpler spectra where transitions of phonons belonging to only one symmetry species are allowed by symmetry and also when both of them appear in the same spectrum.

5 | CONCLUSION

In this study, we propose a reassignment of the E (TO) modes of the *R*3*c* $LiNbO_3$ crystal, in particular for the 2 E and 9 E modes, which have been a matter of discussion in the recent years. The investigation of the vibrational properties of this system was carried out based on a new series of DFT calculations with full periodic boundary conditions, using the CRYSTAL software and the comparison of these results with the polarized Raman experimental spectra of the crystal. This comparison demonstrated the excellent ability of the theoretical approach used to calculate the wavenumbers of the A1 and E (TO) modes. In addition, it was shown that the relative Raman intensities for both types of vibrations in the different experimental configurations are remarkably well predicted. Overall, the present investigation demonstrates that the LCAO approach, as implemented in the CRYSTAL software gives excellent results regarding the calculation of Raman tensors and polarized Raman spectra. The possibility to put in correspondence the individual Raman tensor components and bands intensities in the different back-scattering experimental configurations allowed to demonstrate that the computed Raman tensors are very accurate, considering not only their average values (tensors invariant in the combination suitable for the description of Raman scattering of isotropic materials) but also the tensors individual components.

ACKNOWLEDGMENTS

The authors acknowledge financial support from the Portuguese Science Foundation ("Fundação para a Ciência e a Tecnologia"—FCT)—Projects CQC UIDB/00313/2020 and UIDP/00313/2020, also co-funded by FEDER/COMPETE 2020-EU. Access to instruments from Laser-Lab Coimbra facility funded under QREN-Mais Centro is gratefully acknowledged. B.A.N. also acknowledges FCT for the SFRH/BD/129852/2017 PhD Scholarship.

ORCID

Bernardo A. Nogueira https://orcid.org/0000-0002-1756-377X
Alberto Milani https://orcid.org/0000-0001-6026-5455
Chiara Castiglioni https://orcid.org/0000-0002-6945-9157
Rui Fausto https://orcid.org/0000-0002-8264-6854

REFERENCES

[1] R. S. Weis, T. K. Gaylord, *Appl. Phys. A Solids Surfaces* **1985**, *37*, 191.
[2] P. Hermet, M. Veithen, P. Ghosez, *J. Phys. Condens. Matter* **2007**, *19*, 456202.
[3] K. Buse, A. Adibi, D. Psaltis, *Nature* **1998**, *393*, 665.
[4] L. Hesselink, S. S. Orlov, A. Liu, A. Akella, D. Lande, R. R. Neurgaonkar, *Science* **1998**, *282*, 1089.
[5] I. Noiret, J. Lefebvre, J. Schamps, F. Delattre, A. Brenier, M. Ferriol, *J. Phys. Condens. Matter* **2000**, *12*, 2305.
[6] Y. Repelin, E. Husson, F. Bennani, C. Proust, *J. Phys. Chem. Solids* **1999**, *60*, 819.
[7] R. F. Schaufele, M. J. Weber, *Phys. Rev.* **1966**, *152*, 705.
[8] M. D. Fontana, P. Bourson, *Appl. Phys. Rev.* **2015**, *2*, 040602.
[9] V. Caciuc, A. Postnikov, G. Borstel, *Phys. Rev. B - Condens. Matter Mater. Phys.* **2000**, *61*, 8806.
[10] K. Parlinski, Z. Li, *Phys. Rev. B - Condens. Matter Mater. Phys.* **2000**, *61*, 272.
[11] R. Dovesi, A. Erba, R. Orlando, C. M. Zicovich-Wilson, B. Civalleri, L. Maschio, M. Rérat, S. Casassa, J. Baima, S. Salustro, B. Kirtman, *Wiley Interdiscip. Rev. Comput. Mol. Sci.* **2018**, *8*, e1360.
[12] R. Dovesi, V. R. Saunders, C. Roetti, R. Orlando, C. M. Zicovich-Wilson, F. Pascale, B. Civalleri, K. Doll, N. M. Harrison, I. J. Bush, P. D'Arco, M. Llunell, M. Causà, Y. Noël, L. Maschio, A. Erba, M. Rerat, S. Casassa, CRYSTAL17 User's Manual. Uni.
[13] C. Lee, W. Yang, R. G. Parr, *Phys. Rev. B* **1988**, *37*, 785.
[14] J. Laun, D. V. Oliveira, T. Bredow, *J. Comput. Chem.* **2018**, *39*, 1285.
[15] D. V. Oliveira, J. Laun, M. F. Peintinger, T. Bredow, *J. Comput. Chem.* **2019**, *40*, 2364.
[16] M. F. Peintinger, D. V. Oliveira, T. Bredow, *J. Comput. Chem.* **2013**, *34*, 451.
[17] S. C. Abrahams, J. M. Reddy, J. L. Bernstein, *J. Phys. Chem. Solids* **1966**, *27*, 997.
[18] S. Dall'Olio, R. Dovesi, R. Resta, *Phys. Rev. B - Condens. Matter Mater. Phys.* **1997**, *56*, 10105.
[19] R. Dovesi, R. Orlando, A. Erba, C. M. Zicovich-Wilson, B. Civalleri, S. Casassa, L. Maschio, M. Ferrabone, M. De La Pierre, P. D'Arco, Y. Nöel, M. Causa, M. Rerat, B. Kirtman, *Int. J. Quantum Chem.* **2014**, *114*, 1287.
[20] B. Montanari, B. Civalleri, C. M. Zicovich-Wilson, R. Dovesi, *Int. J. Quantum Chem.* **2006**, *106*, 1703.
[21] F. Pascale, M. Catti, A. Damin, R. Orlando, V. R. Saunders, R. Dovesi, *J. Phys. Chem. B* **2005**, *109*, 18522.
[22] F. Pascale, C. M. Zicovich-Wilson, F. López Gejo, B. Civalleri, R. Orlando, R. Dovesi, *J. Comput. Chem.* **2004**, *25*, 888.
[23] C. M. Zicovich-Wilson, F. Pascale, C. Roetti, V. R. Saunders, R. Orlando, R. Dovesi, *J. Comput. Chem.* **2004**, *25*, 1873.
[24] G. Keresztury, Raman spectroscopy, in *Theory in Handbook of Vibrational Spectroscopy*, (Ed: J. M. Chalmers), John Wiley & Sons, Ltd, Chichester **2006**.
[25] R. Loudon, *Adv. Phys.* **1964**, *13*, 423.
[26] J. Kim, J. U. Lee, H. Cheong, *J. Phys. Condens. Matter* **2020**, *32*, 343001.
[27] H. Kuzmany, *Solid-State Spectroscopy*, Springer, Berlin **1998**.
[28] A. S. Barker, R. Loudon, *Phys. Rev.* **1967**, *158*, 433.
[29] R. Claus, G. Borstel, E. Wiesendanger, L. Steffan, *Phys. Rev. B* **1972**, *6*, 4878.
[30] V. S. Gorelik, P. P. Sverbil, *Inorg. Mater.* **2015**, *51*, 1104.
[31] I. P. Kaminow, W. D. Johnston, *Phys. Rev.* **1967**, *160*, 519.

[32] A. Ridah, P. Bourson, M. D. Fontana, G. Malovichko, *J. Phys. Condens. Matter* **1997**, *9*, 9687.
[33] X. Yang, G. Lan, B. Li, H. Wang, *Phys. Status Solidi* **1987**, *142*, 287.

SUPPORTING INFORMATION

Additional supporting information may be found online in the Supporting Information section at the end of this article.

How to cite this article: Nogueira BA, Milani A, Castiglioni C, Fausto R. The correlation between experimental polarized Raman spectra and their density functional theory prediction in the LCAO framework: The *R*3*c* $LiNbO_3$ crystal as a test case. *J Raman Spectrosc*. 2021;52:995–1010. https://doi.org/10.1002/jrs.6091